

# Timing of the Meso-Tethys Ocean opening: Evidence from Permian sedimentary provenance changes in the South Qiangtang Terrane, Tibetan Plateau



Jian-Jun Fan <sup>a,b,\*</sup>, Yaoling Niu <sup>b</sup>, An-Bo Luo <sup>a</sup>, Chao-Ming Xie <sup>a</sup>, Yu-Jie Hao <sup>c</sup>, Hai-Yong Liu <sup>d</sup>

<sup>a</sup> College of Earth Sciences, Jilin University, Changchun 130061, PR China

<sup>b</sup> Department of Earth Sciences, Durham University, Durham DH1 3LE, UK

<sup>c</sup> Key Laboratory of Mineral Resources Evaluation in Northeast Asia, Ministry of Natural Resources of China, Changchun, 130061, PR China

<sup>d</sup> College of Earth Sciences, Chengdu University of Technology, Chengdu 610059, PR China

## ARTICLE INFO

### Keywords:

Detrital zircon

Rifting

Indian margin of Gondwana

## ABSTRACT

Timing of the opening of the Meso-Tethys Ocean, represented by the Bangong–Nujiang Suture Zone on the Tibetan Plateau, remains controversial. Further research is required to understand the breakup of the northern Gondwana margin and the tectonic evolution of the Tethyan realm. In this study, we present petrography, U-Pb dating and Hf isotopic data for detrital zircons from Upper Carboniferous–Upper Permian strata in the South Qiangtang Terrane on the Tibetan Plateau. These data, together with data from previous literature, indicate a youngest detrital zircon age peak of ca. 550 Ma for Upper Carboniferous–Lower Permian strata. This is far older than the depositional age of ca. 300 Ma and indicates a source in the stable Gondwana Continent. Upper Permian strata yield younger ages (490–247 Ma) with peaks at ca. 460, 355, 290 and 260 Ma, indicating a source in the active South Qiangtang Terrane. Combined with the unconformity between the Lower and Upper Permian strata in the western South Qiangtang Terrane, we conclude that a significant change in sedimentary provenance occurred at 280–260 Ma. This provenance change might have resulted from the 300–279 Ma rifting magmatism on the northern Indian margin of Gondwana (e.g., South Qiangtang). The 300–279 Ma magmatism is interpreted to reflect the early stages of rifting, and the subsequent 280–260 Ma sedimentary provenance change is interpreted as the later stage, both of which established a complete Early–Middle Permian (300–260 Ma) rifting process that marks the opening of the Meso-Tethys Ocean.

## 1. Introduction

The Meso-Tethys Ocean, which is represented by the Bangong–Nujiang Suture Zone (BNSZ) on the central Tibetan Plateau, places important constraints on the Mesozoic tectonic history of the Tibetan Plateau (Kapp et al., 2007; Pan et al., 2012; Zhang et al., 2014a; Zhu et al., 2016), and provides insights into widespread late Mesozoic mineralization within central Tibet (Geng et al., 2016; Li et al., 2018). Although the BNSZ has been studied extensively (Allègre et al., 1984; Yin and Harrison, 2000; Kapp et al., 2007; Shi et al., 2008; Pan et al., 2012; Zhang et al., 2014a, 2014b, 2017, 2019; Li et al., 2014, 2018, 2019, 2020; Zhu et al., 2016; Wang et al., 2016; Zeng et al., 2016; Hu et al., 2017; Liu et al., 2017; Chen et al., 2017; Ma et al., 2017; Fan et al., 2018, 2021; Wu et al., 2018; Hao et al., 2019; Tang et al., 2020; Luo

et al., 2020), many aspects of the evolution of the Meso-Tethys Ocean remain controversial, and the timing of the opening of the Meso-Tethys Ocean has been subject to fierce debate (Metcalfe, 2013; Zhai et al., 2013; Liao et al., 2015; Chen et al., 2017; Liu et al., 2017; Fan et al., 2017; Wang et al., 2019; Zhang et al., 2019; Li et al., 2019).

An understanding of the timing of opening of the Meso-Tethys Ocean is critical for constraining the history of the breakup of the northern Gondwana margin, and for understanding the tectonic evolution of the Tethyan realm. The opening of the Meso-Tethys Ocean is associated with Carboniferous–Permian rifting of the South Qiangtang Terrane from the Indian margin of Gondwana (Metcalfe, 2013; Zhai et al., 2013; Liao et al., 2015; Chen et al., 2017; Liu et al., 2017; Fan et al., 2017; Wang et al., 2019; Zhang et al., 2019; Li et al., 2019); therefore, the Carboniferous–Permian strata in the South Qiangtang Terrane (Fig. 1b) are

\* Corresponding author.

E-mail addresses: [fanjj03@163.com](mailto:fanjj03@163.com) (J.-J. Fan), [yaoling.niu@durham.ac.uk](mailto:yaoling.niu@durham.ac.uk) (Y. Niu).

expected to provide crucial information on the timing of the Meso-Tethys opening.

In this paper, in order to discuss the timing of the Meso-Tethys opening, we examine the Upper Carboniferous–Upper Permian strata (Fig. 1b) in the South Qiangtang Terrane by using a combined approach of detailed petrographic analysis, detrital zircon U–Pb dating, and Hf isotope analysis. The resultant data allow us to identify a significant change in sedimentary provenance during 280–260 Ma in the South Qiangtang Terrane, which is interpreted as the sedimentary and tectonic response to continental rifting, the precursory process of the Meso-

Tethys Ocean opening. This work thus establishes an important framework for the timing of opening of the Meso-Tethys Ocean.

## 2. Upper Carboniferous–Upper Permian strata in the South Qiangtang Terrane

From south to north, the Tibetan Plateau is made up of the Himalaya, Lhasa, South Qiangtang, North Qiangtang, Songpan-Ganzi-Hoh Xil and Qaidam terranes (Fig. 1a). These terranes are separated by five suture zones (Fig. 1a; Allègre et al., 1984; Yin and Harrison, 2000; Pan et al.,

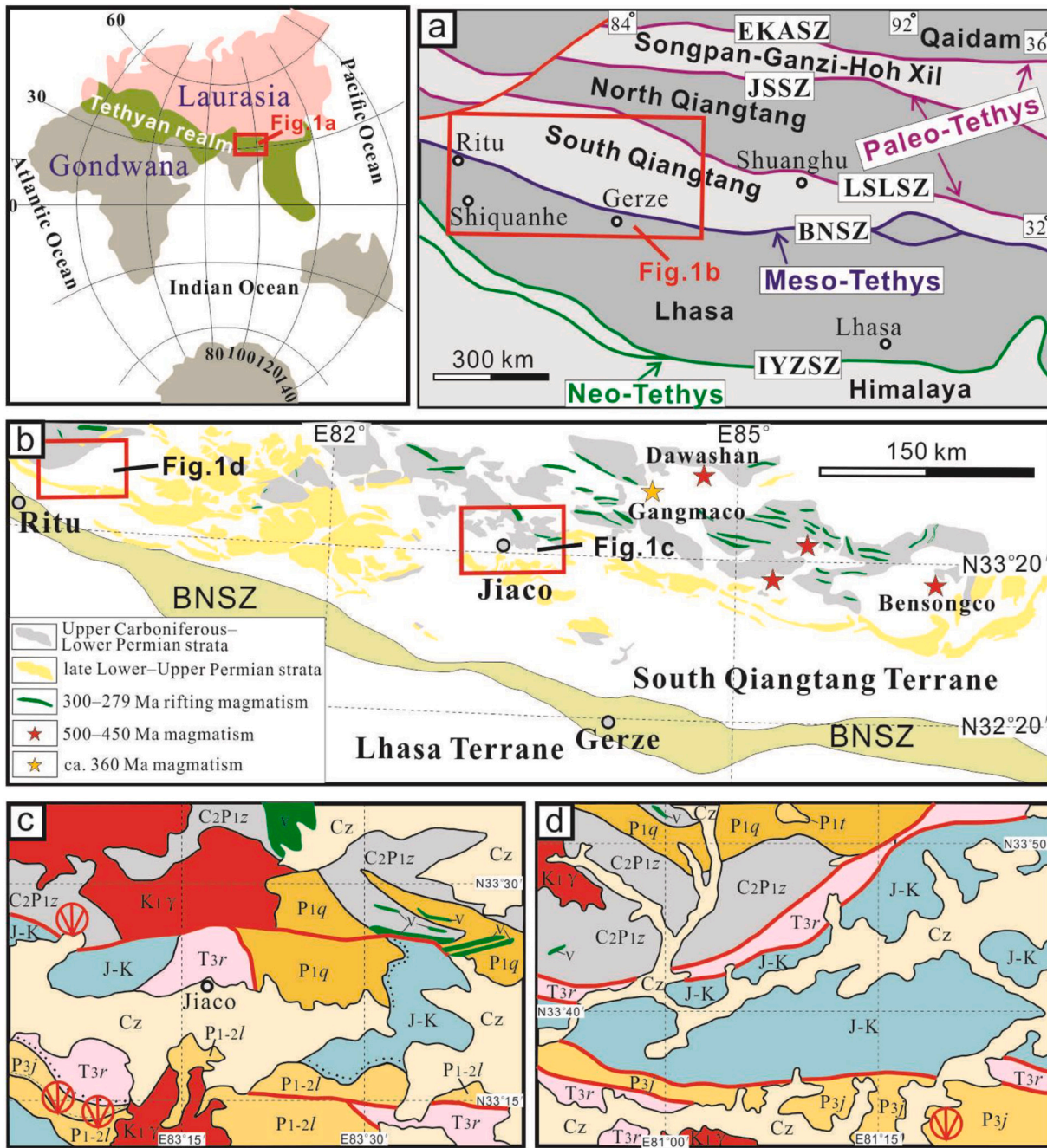


**Fig. 1.** (a) Tectonic framework of the Tibetan Plateau. EKASZ, East Kunlun–A'nyemaqen Suture Zone; JSSZ, Jinshajiang Suture Zone; LSLSZ, Longmuco–Shuanghu–Lancangjiang Suture Zone; BNSZ, Bangong–Nujiang Suture Zone; IYZSZ, Indus–Yarlung Zangbo Suture Zone. (b) Geological map of central Tibet showing the Upper Carboniferous–Upper Permian strata. (c) Geological map of the Jiaco area. (d) Geological map of the Ritu area. Cz, Cenozoic; J-K, Jurassic–Cretaceous strata; T<sub>3</sub>r, Upper Triassic Riganpeco Formation; P<sub>3</sub>j, Upper Permian Jipuria Formation; P<sub>1-2l</sub>, Lower–Middle Permian Lugu Formation; P<sub>1</sub>t, Lower Permian Tulonggongba Formation; P<sub>1</sub>q, Lower Permian Qudi Formation; C<sub>2</sub>P<sub>1z</sub>, Upper Carboniferous–Lower Permian Zhanjin Formation; K<sub>1</sub>γ, Early Cretaceous granitoids; v, 300–279 Ma mafic dike swarms.

2012; Metcalfe, 2013; Zhu et al., 2013; Xu et al., 2015; Zhai et al., 2016). This study focuses on the Jiaco and Ritu areas in the middle and western South Qiangtang Terrane, respectively (Fig. 1b), where Upper Carboniferous–Upper Permian strata are widely distributed within complex sedimentary sequences (Figs. 1c, d, 2).

The Upper Carboniferous–Upper Permian strata in the Jiaco area include the Zhanjin, Qudi, Lugu and Jipuria formations (Figs. 1c, 2), and those in the Ritu area include the Zhanjin, Qudi, Tunlonggongba, Longge and Jipuria formations (Figs. 1d, 2).

The Zhanjin Formation is dominated by grey-green glacial marine diamictite (Fig. 3a)—formed by the Late Carboniferous–Early Permian Gondwanan glaciation (Jin, 2002; Fielding et al., 2008; Zhang et al., 2013; Fan et al., 2015)—sandstone, siltstone and shale. Sakmarian bivalves (e.g., *Eurydesma perversum*) and solitary corals (e.g., *Cyathaxonia* and *Lophophyllidium*; Liang et al., 1983; Liu and Cui, 1983; Zhang et al., 2013) in the sandstone and siltstone also indicate a Late Carboniferous–Early Permian age. Slump structures, convolute bedding and Bouma sequences are common in the Zhanjin Formation, indicating a bathyal to abyssal depositional environment (Fan et al., 2015; Zhang et al., 2019). The overlying Qudi Formation is dominated by littoral–neritic sandstone in the western South Qiangtang Terrane, and bathyal to abyssal siltstone and shale in the middle South Qiangtang Terrane (Zhang et al., 2012a, 2019). This Formation contains fusulines (e.g., *Pseudofusulina*, *Chalaroschwagerina*, *Pamirina*) of Early Permian age

(Zhang et al., 2012a, 2013). The Lugu Formation in the middle South Qiangtang Terrane is dominated by basalt and littoral–neritic limestone; Early Permian fusulines (*Cancellina*, *Parafusulina* and *Pseudodoloiolina*) occur in the basal strata, and Middle Permian *Neoschwagerina* and *Verbeekina* occur in the upper strata of the formation (Nie and Song, 1983a; Zhang et al., 2012a, 2013, 2019). The Tunlonggongba and Longge formations in the western South Qiangtang Terrane are both dominated by littoral–neritic limestone. The Tunlonggongba Formation contains the fusuline *Monodiexodina*, indicating a late Early Permian age (Nie and Song, 1983b). The Longge Formation contains the coral *Iranophyllum*, and the fusulines *Neoschwagerina*, *Dunbarula*, *Sumatrina*, *Chusenella* and *Kahlerina* of late Middle Permian age (Liang et al., 1983; Nie and Song, 1983c; Zhang et al., 2013). The nature of the stratigraphic contact between the Tunlonggongba and Longge formations is unclear, because the Longge Formation occurs as ‘blocks’ in the western South Qiangtang Terrane (Zhang et al., 2019). The Jipuria Formation is dominated by littoral–neritic conglomerate, sandstone, siltstone and limestone, with minor andesite and tuff (Figs. 2, 3b; Liang et al., 1983; Xia and Liu, 1997; Mou et al., 2010; Zhang et al., 2013, 2019). This formation overlies the Tunlonggongba Formation with angular unconformity in the western South Qiangtang Terrane, whereas it overlies the Lugu Formation with parallel unconformity in the central South Qiangtang Terrane (Fig. 2). In the western South Qiangtang Terrane, the Jipuria Formation contains the fusulines *Codonofusiella*, *Reichelina* and *Palaeofusulina*, the corals

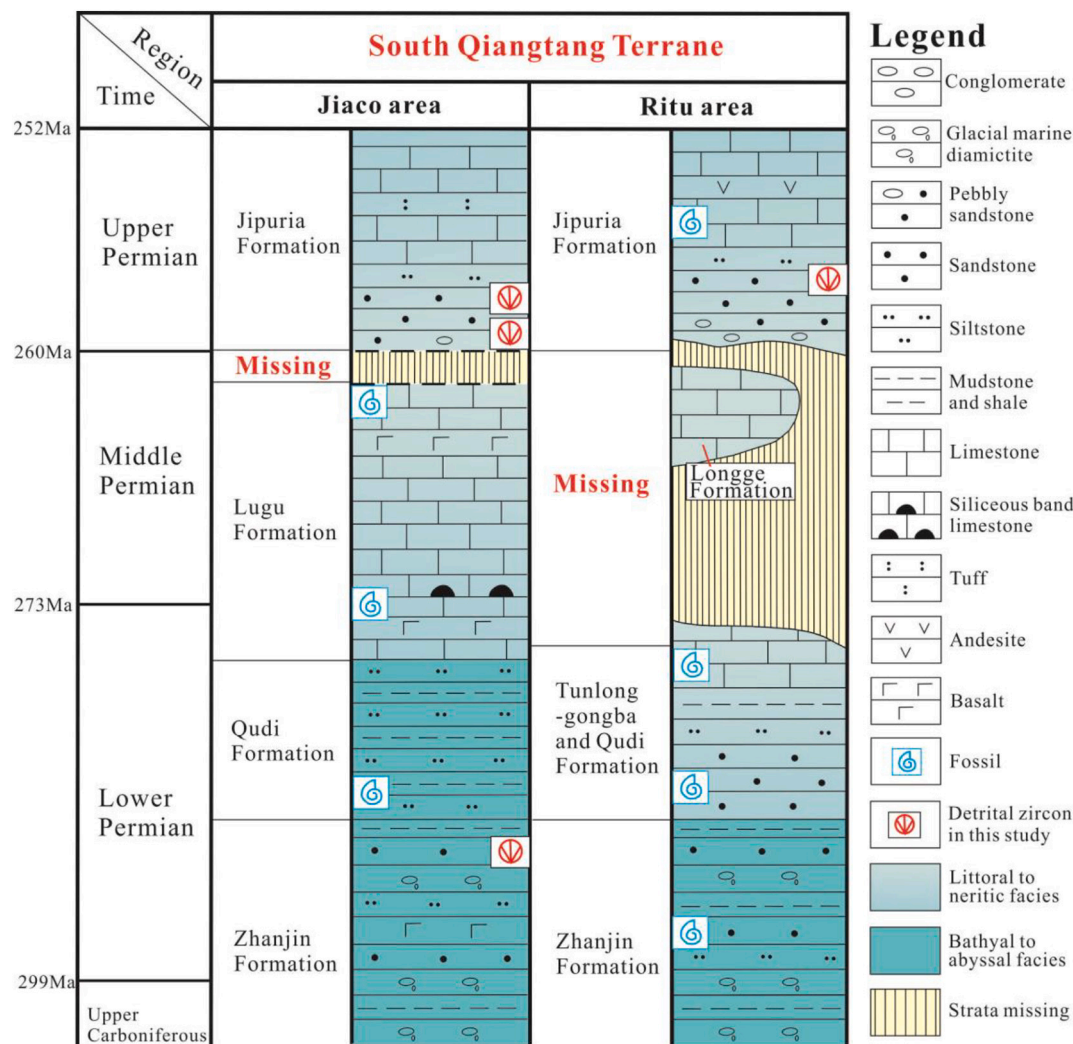
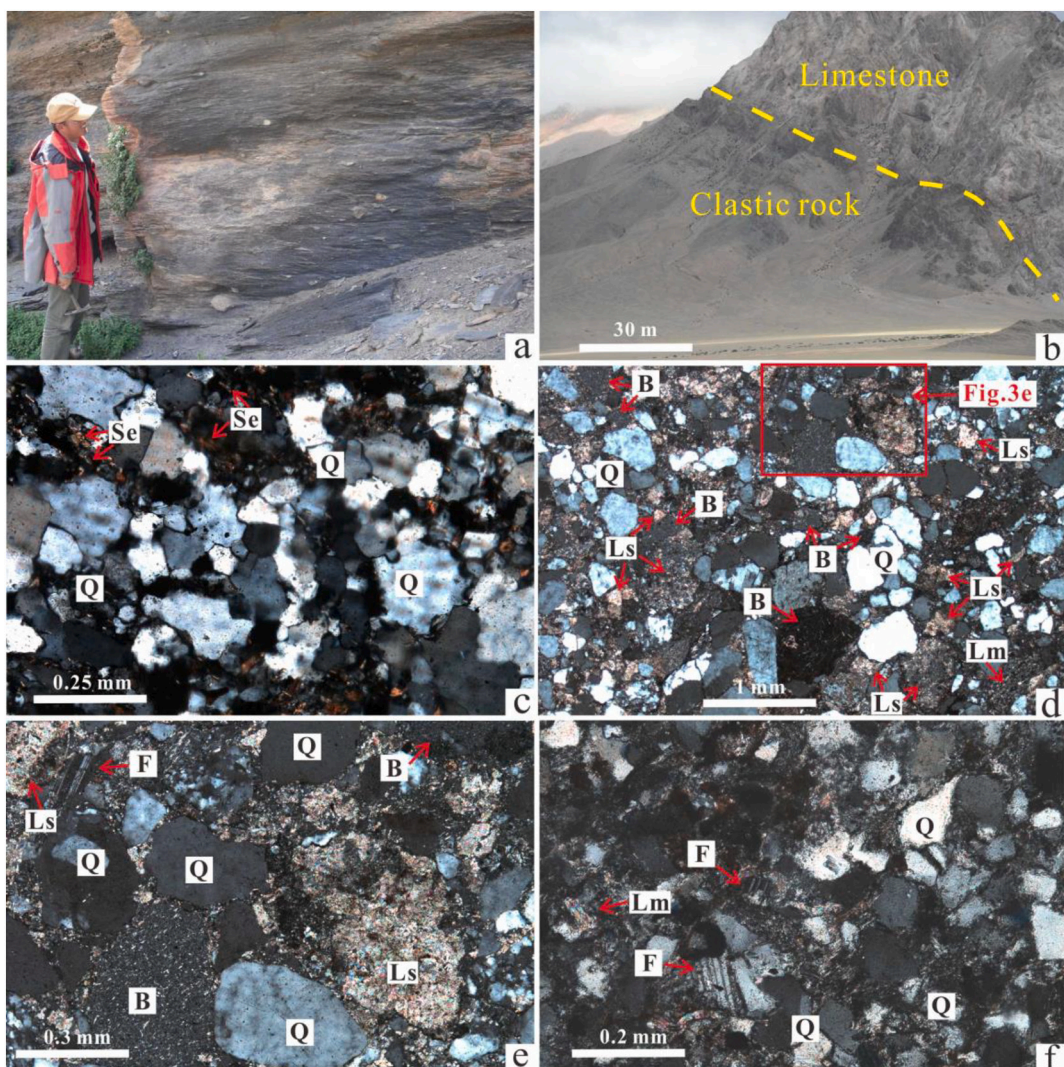


Fig. 2. Stratigraphic columns for the Upper Carboniferous–Upper Permian strata in the Jiaco and Ritu areas of the South Qiangtang Terrane (modified after Liang et al., 1983; Mou et al., 2010; Zhang et al., 2013, 2019).



**Fig. 3.** (a) Upper Carboniferous–Lower Permian glacial marine diamictite in the South Qiangtang Terrane. (b) Clastic rocks and limestones of the Upper Permian Jipuria Formation in the South Qiangtang Terrane. (c) Photomicrograph of Upper Carboniferous–Lower Permian sandstone in the Jiaco area. (d–e) Photomicrographs of Upper Permian sandstone in the Jiaco area. (f) Photomicrograph of Upper Permian sandstone in the Ritu area. Ls, limestone lithic fragments; B, basalt lithic fragments; Lm, metamorphic lithic fragments; Q, quartz; F, feldspar; Se, Sericite.

*Waagenophyllum* and *Lophophyllidium*, and the brachiopods *Permeicodothyris* and *Leptodus*, all indicating a Late Permian age (Wu and Lan, 1990; Zhang et al., 2013). Due to an absence of fossils, the age of the Jipuria Formation in the middle South Qiangtang Terrane remains unconstrained.

### 3. Analytical methods

#### 3.1. Sandstone petrographic analysis

Sandstone samples from the Upper Carboniferous–Lower Permian Zhanjin Formation and the Upper Permian Jipuria Formation in the South Qiangtang Terrane were prepared and studied using petrographic analysis. Modal analysis was carried out on Upper Permian samples that exhibit minor metamorphism. Approximately 300 grains were identified and counted in each sample, following the Gazzi-Dickinson method (Dickinson, 1985); crystals or grains larger than ~60 µm in diameter within rock fragments were counted as single minerals (Ingersoll et al., 1984). The results are presented in Supplementary Table S1.

#### 3.2. Zircon U–Pb dating

Based on field work, four sandstone samples were selected for U–Pb dating: one from the Upper Carboniferous–Lower Permian Zhanjin Formation in the Jiaco area (sampled S19T21, 33°31'31"N, 83°13'16"E, 5323 m elevation), two from the Upper Permian Jipuria Formation in the Jiaco area (sampled D18T16, 33°13'40"N, 83°9'17"E, 4926 m, elevation; and D18T17, 33°8'24"N, 83°17'49"E, 4622 m elevation), and one from the Upper Permian Jipuria Formation in the Ritu area (sampled B19T17, 33°34'35"N, 80°18'4"E, 4482 m elevation).

Zircon grains were extracted from sandstone samples by crushing and using a combined method of heavy liquid and magnetic separation in the Laboratory of the Geological Team of Hebei Province, Langfang, China. Internal structures of the grains were imaged using cathodoluminescence (CL) in the Continental Dynamics Laboratory, Chinese Academy of Geological Sciences, Beijing, China to select spots for laser ablation–inductively coupled plasma–mass spectroscopy (LA–ICP–MS) analysis. The LA–ICP–MS U–Pb zircon dating was carried out in the Key Laboratory of Mineral Resources Evaluation in Northeast Asia, Ministry of Natural Resources of China, Changchun, China. The spot size was 32 µm for each sample. Helium was used as a carrier gas. The reference zircon standards 91500 (Wiedenbeck et al., 1995) and NIST610 ( $^{29}\text{Si}$ )

were used for instrumental calibration. The Pb correction method of Anderson (2002) was applied, with analytical details following those described by Yuan et al. (2004). Reported uncertainties for the age analyses are given as  $1\sigma$  values with weighted mean ages at the 95% confidence level. Isotopic data were processed using the GLITTER (version 4.4) and Isoplot/Ex (version 3.0) programs (Ludwig, 2003). Reported ages are  $^{206}\text{Pb}/^{238}\text{U}$  ages for grains  $< 1000$  Ma and  $^{207}\text{Pb}/^{206}\text{Pb}$  ages for grains  $> 1000$  Ma. For statistical purposes, zircon ages with  $<10\%$  discordance are used in our discussion.

### 3.3. In situ zircon Hf isotope analysis

Twelve zircons from the Upper Permian sandstone samples (D18T16, D18T17, and B19T17) were analyzed for Hf isotopic compositions. The same dating spots were used for Hf analysis. The Hf isotope data were collected using a NEPTUNE Plus multi-collector (MC)-ICP-MS at the Beijing Createch Testing Technology Co., Ltd., Beijing, China. A single spot ablation mode with a spot size of  $44 \mu\text{m}$  was used to acquire the data. Each measurement consisted of 20 s of background signal acquisition followed by 50 s of ablation signal acquisition, with analytical processes following those described by Hu et al. (2012). Off-line selection, signals integration of analyte, and mass bias calibrations were performed using the ICP-MS DataCal program (Liu et al., 2010). The

analyzed  $^{176}\text{Hf}/^{177}\text{Hf}$  ratios for the zircon standard (91500) were  $0.282299 \pm 31$  ( $2\sigma_{\text{n}}$ ,  $n=40$ ), which are in agreement with the recommended value within error ( $^{176}\text{Hf}/^{177}\text{Hf}$  ratios of  $0.282302 \pm 8$  at  $2\sigma$ ; Goolaerts et al., 2004; Woodhead et al., 2004).

## 4. Results

### 4.1. Sandstone petrography

Sandstone samples from the Upper Carboniferous–Lower Permian Zhanjin Formation in the Jiaco area have undergone lower greenschist facies metamorphism, causing alteration of the muddy matrix into sericite (Fig. 3c). The samples are dominated by quartz grains ( $>95\%$ ; Fig. 3c). However, sandstone samples from the Upper Permian Jipuria Formation in the Jiaco area are dominated by poorly sorted quartz grains (76%–83%) and lithic fragments (12%–21%; Table S1). The lithic fragments comprise mainly limestone and basalt (Fig. 3d–e).

Sandstone samples from the Upper Permian Jipuria Formation in the Ritu area are dominated by fine-grained ( $<0.1 \text{ mm}$ ) quartz grains (77%–83%), feldspar (8%–12%) and lithic fragments (9%–14%; Table S1, Fig. 3f). Polysynthetic twinning is common in the feldspar (Fig. 3f), and lithic fragments composed predominantly of metamorphic and volcanic detritus (Table S1).

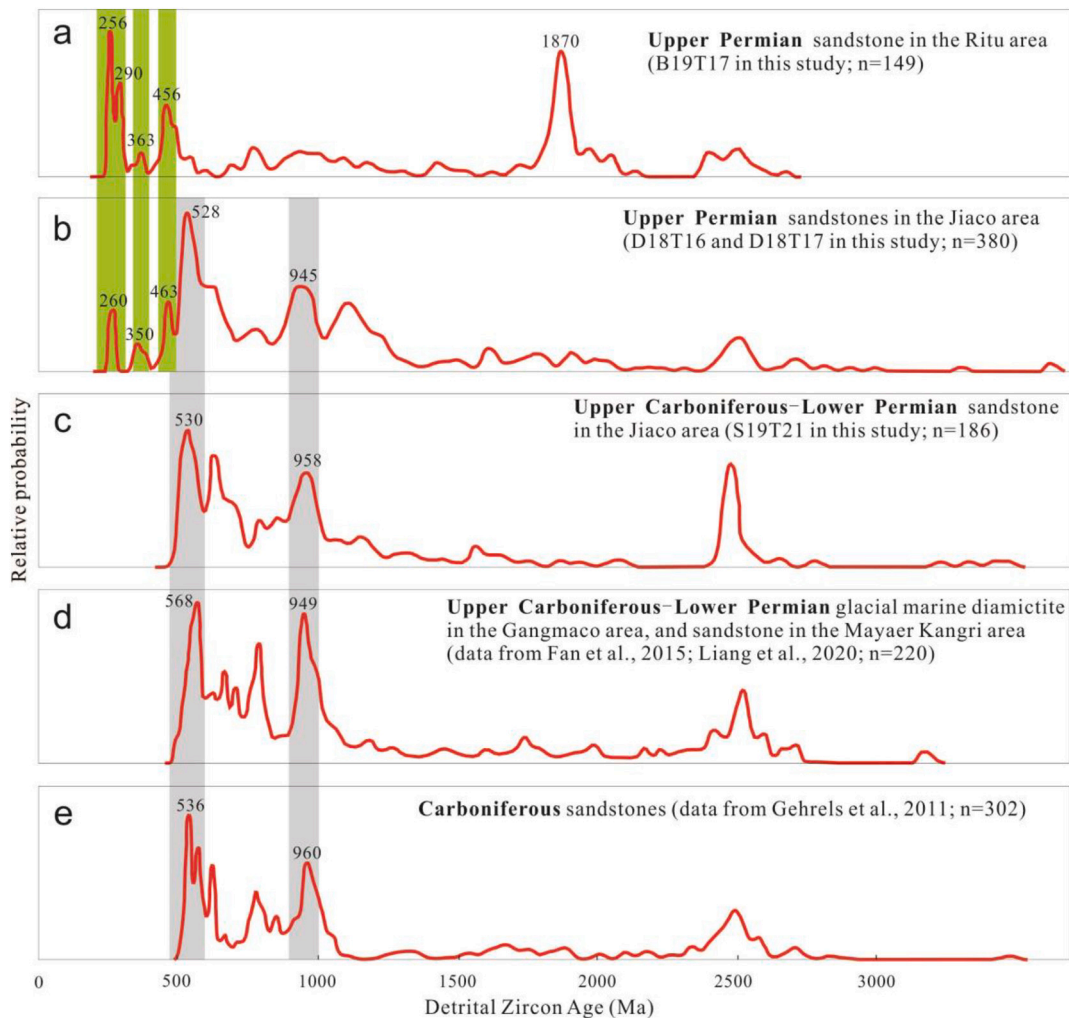


**Fig. 4.** Summary of detrital zircon age distributions of the Carboniferous–Permian sandstones of this study and previous work (Gehrels et al., 2011; Liang et al., 2020) in the South Qiangtang Terrane. Similar main age peaks between Carboniferous and Permian strata are shown in grey bands, whereas different age peaks are shown in green bands.  $n =$  total number of analyses. (For interpretation of the references to colour in this figure legend, the reader is referred to the web version of this article.)

#### 4.2. Zircon U—Pb dating

Representative cathodoluminescence (CL) images of detrital zircons are presented in Fig. S1, and age data are presented in Tables S2–S4.

Detrital zircon ages from one Upper Carboniferous–Lower Permian sandstone sample from the Zhanjin Formation from the Jiaco area (S19T21; Fig. 1c) range from 3944 to 498 Ma, with two main peaks at ca. 958 and ca. 530 Ma (Fig. 4c). These age distributions are in good agreement with those of detrital zircons from Carboniferous–Lower Permian strata in other areas of the South Qiangtang Terrane (Fig. 4d–e).

Detrital zircon ages from two Upper Permian sandstone samples from the Jipuria Formation from the Jiaco area (Fig. 1c) yield a similar range of ages from 3630 to 247 Ma, with five main peaks at ca. 945, 528, 463, 350, and 260 Ma (Fig. 4b). Detrital zircon ages from one Upper Permian sandstone sample from the Jipuria Formation in the Ritu area (B19T17; Fig. 1d) range from 2664 Ma to 247 Ma, with five main peaks at ca. 1870, 456, 363, 290, and 256 Ma (Fig. 4a). These age distributions are significantly different from those of the Carboniferous–Lower Permian strata in the South Qiangtang Terrane (Fig. 4).

#### 4.3. Zircon Hf isotope data

Zircon Hf isotope data are presented in Table S5. Detrital zircons with ages of 285–248 Ma from the Upper Permian sandstone samples from the Jipuria Formation have  $\epsilon\text{Hf(t)}$  values of  $-15.1$  to  $+12.5$ , with TDM<sub>2</sub> ages (two-stage Hf model ages) in the range of 489–2241 Ma (Fig. 5).

### 5. Discussion

#### 5.1. Age of the Jipuria Formation in the South Qiangtang Terrane

The age of the Jipuria Formation in the Jiaco area of the middle South Qiangtang Terrane is currently unconstrained, owing to a lack of fossils. Andesite and pyroclastic rocks in the Jipuria Formation indicate magmatic eruptions occurred during deposition of the formation (Liang et al., 1983; Xia and Liu, 1997; Mou et al., 2010; Fig. 2); therefore, the depositional age of the Jipuria Formation should be close to the youngest zircon age (Malusa et al., 2011; Cawood et al., 2012; von Eynatten and Dunkl, 2012). To reasonably constrain the depositional age of the Jipuria Formation, we used the mean age of the youngest three or more

grains that overlap in age at  $2\sigma$  ( $\text{YC}2\sigma$ ). This method has proved effective in sandstones from the Colorado Plateau (Dickinson and Gehrels, 2009). In the Jiaco area, sandstone samples from the Jipuria Formation yield Late Permian  $\text{YC}2\sigma$  ages of  $259 \pm 11$  Ma ( $n = 5$ ) and  $257 \pm 11$  Ma ( $n = 5$ ), which are similar to those of the Jipuria Formation in the Ritu area ( $\text{YC}2\sigma = 255 \pm 8$  Ma,  $n = 10$ ; Fig. S2). These  $\text{YC}2\sigma$  ages (259–255 Ma), together with Late Permian fossils reported in the Ritu area (Wu and Lan, 1990; Zhang et al., 2013), provide strong evidence that the Jipuria Formation in the South Qiangtang Terrane is of Upper Permian age.

#### 5.2. Provenance analysis: a 280–260 Ma sedimentary provenance change in the South Qiangtang Terrane

Prior to provenance analysis, it is necessary to consider the paleo-position of the South Qiangtang Terrane during the Carboniferous–Permian. The glacial marine diamictites (Fig. 3a) that formed as a result of the Late Carboniferous–Early Permian Gondwanan glaciation (ca. 300 Ma; Jin, 2002; Fielding et al., 2008; Zhang et al., 2013; Fan et al., 2015) are widespread in the South Qiangtang Terrane (Fan et al., 2015). This indicates that the South Qiangtang Terrane was located near the Gondwana Continent during the Late Carboniferous–Early Permian period. The distinctive ca. 950 Ma age peak observed in the Carboniferous–Lower Permian strata (Fig. 4) in the South Qiangtang Terrane is consistent with the emplacement of the 990–900 Ma granitoids of the Indian margin of Gondwana (Zhu et al., 2013). These observations, together with the similarities between the Early Permian fossils (Zhang et al., 2012a, 2012b, 2013, 2014b) and magmatic activity (e.g., the 300–260 Ma mafic magmatism; Zhai et al., 2013; Wang et al., 2019) of the South Qiangtang Terrane and the northern Indian margin of Gondwana (i.e., the Himalayas; Shellnutt et al., 2014) indicate that the South Qiangtang Terrane was part of the northern Indian margin of Gondwana during the Carboniferous–Early Permian (Zhang et al., 2012a; Zhu et al., 2013; Metcalfe, 2013; Zhai et al., 2013; Liao et al., 2015; Chen et al., 2017).

Paleogeographic analysis indicates that the Indian margin of Gondwana was an erosional zone, and the South Qiangtang Terrane was in a passive margin depositional setting during the Late Carboniferous–Early Permian (Fan et al., 2015). The Indian margin of Gondwana may therefore be the source of the Upper Carboniferous–Lower Permian deposits in the South Qiangtang Terrane (Fan et al., 2015). The youngest zircon age peak of ca. 550 Ma in the Upper Carboniferous–Lower Permian strata is far older than the depositional age (ca. 300 Ma; Fig. 4c–d), and thus provides strong evidence for the stable Indian margin of Gondwana source.

The presence of abundant angular to subangular volcanic (e.g., basalts) and sedimentary (e.g., limestones) lithic fragments in the Upper Permian sandstone of the South Qiangtang Terrane (Fig. 3d–e) indicate that their provenance lies in a tectonically active rather than stable setting such as the Indian margin of Gondwana. In addition, these samples plot in the recycled orogen sector in quartz–feldspar–lithic fragment (QFL) and monocrystalline quartz–feldspar–total lithic fragments (QmFLt) discrimination diagrams (Fig. 6). Moreover, many detrital zircons in the Upper Permian sandstone of the South Qiangtang Terrane yield ages (490–247 Ma) with peaks at ca. 460, 355, 290 and 260 Ma, which are not observed in the age spectra of the Carboniferous–Lower Permian sandstones (Figs. 4, 7). These observations provide evidence that a significant sedimentary provenance change occurred between the Carboniferous–Early Permian and the Late Permian in the South Qiangtang Terrane.

Lithic fragments in the Upper Permian sandstone are mostly poorly sorted, and are angular to subangular in shape (Fig. 3d–e), indicating near-source deposition. Lithic fragments in the Upper Permian sandstone in the Jiaco area are dominated by limestone and basalt (Fig. 3d–e), similar to that observed in the rocks of the Lower–Middle Permian Lugu Formation in the South Qiangtang Terrane (Fig. 2; Zhang et al., 2012a). Detrital zircons (299–285 Ma) in the Upper Permian

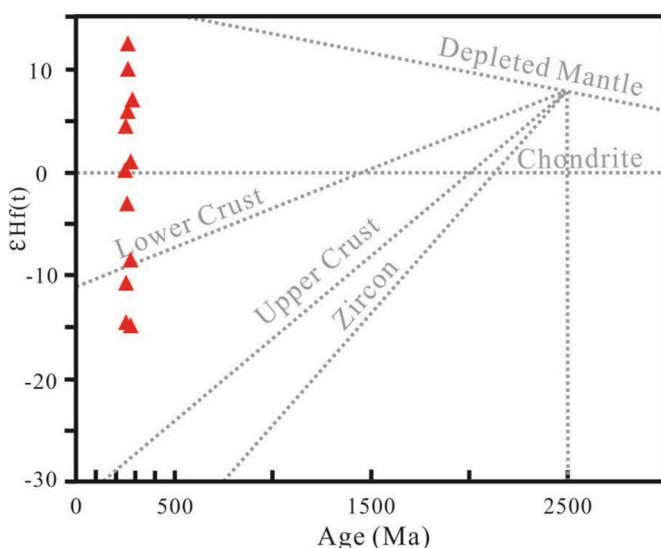
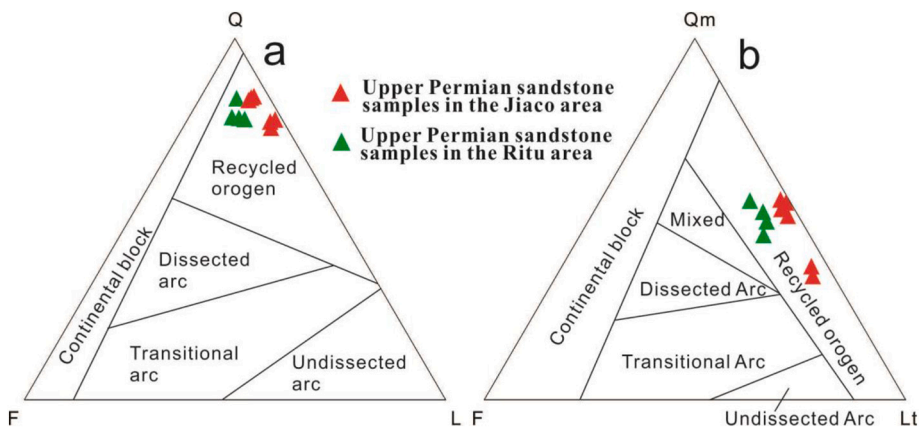
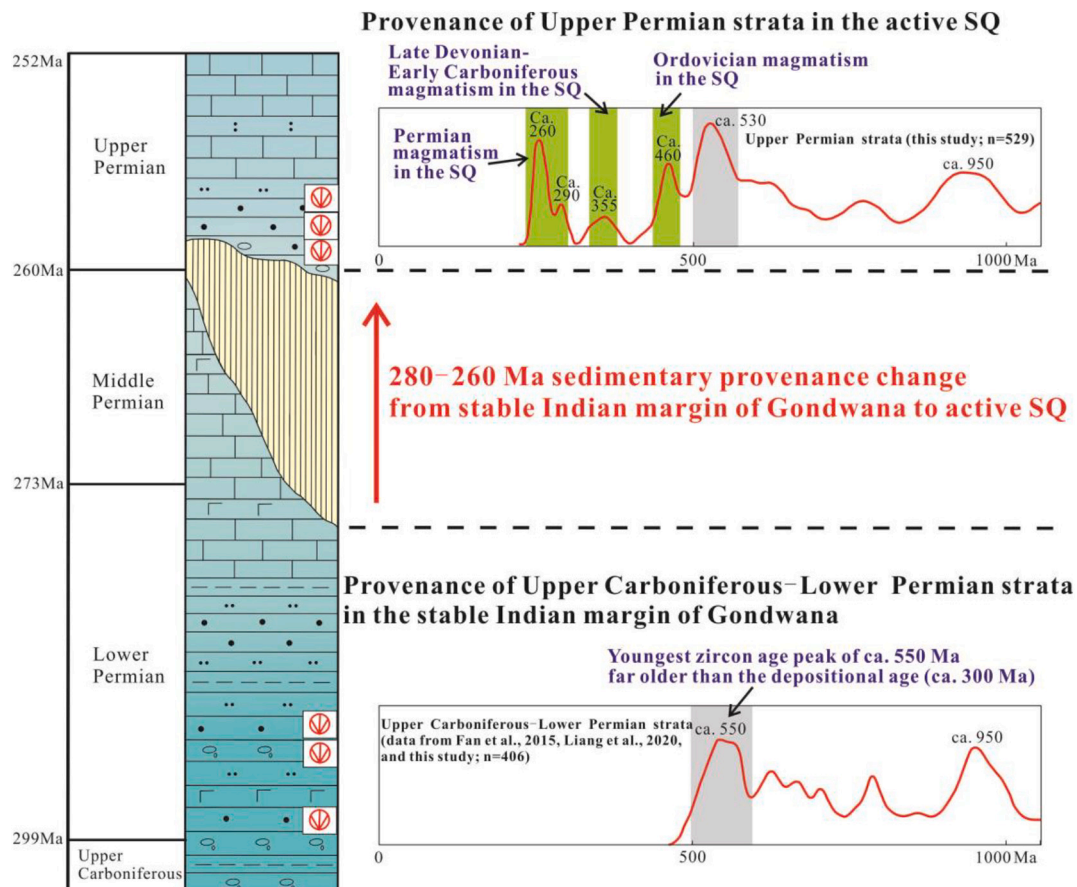


Fig. 5. Zircon  $\epsilon\text{Hf(t)}$  values of the youngest detrital zircons (285–248 Ma) from the Upper Permian sandstones versus age diagram.



**Fig. 6.** Dickinson ternary diagrams for the Upper Permian sandstones in the South Qiangtang Terrane.



**Fig. 7.** Comprehensive diagram showing the 280–260 Ma sedimentary provenance change in the South Qiangtang Terrane. SQ, South Qiangtang Terrane. Legends are the same as in Fig. 2.

sandstone in the Ritu area mostly exhibit weak and broad zoning in CL images (Fig. S1), and the detrital zircon grain with an age of 285 Ma has a  $\epsilon\text{Hf}$  ( $t$ ) value of +6.9 (Table S5), both of which are similar to those of the 300–279 Ma mafic rocks (e.g., mafic dike swarms, +4.2 to +15.8; Fig. 1b; Zhai et al., 2013; Wang et al., 2019) in the South Qiangtang Terrane. In the Upper Permian sandstone, the 490–445 Ma zircon ages with a peak at ca. 460 Ma, and the 384–334 Ma zircon ages with a peak at ca. 355 Ma (Fig. 7) indicate Ordovician and Late Devonian–Early Carboniferous magmatism occurred in the source region. This corresponds with the magmatism in the South Qiangtang Terrane (Fig. 1b); for example, magmatism occurred at 500–450 Ma in a 300 km-long belt

from Bensongco in the east to Dawashan in the west (Fig. 1b; Hu et al., 2015; Xie et al., 2017; Liu et al., 2019; Xu et al., 2020), and the 360–350 Ma magmatism occurred in the Gangmuco area in the South Qiangtang Terrane (Fig. 1b; Wang et al., 2015a). These observations, together with the basal unconformity of the Upper Permian Jiapuria Formation (Fig. 2) that indicates uplift and erosion of the South Qiangtang Terrane, provide strong evidence that the source of the Upper Permian sandstone is derived from the erosion of sedimentary and magmatic rocks in the South Qiangtang Terrane.

In conclusion, the source of the Upper Carboniferous–Lower Permian strata in the South Qiangtang Terrane lies in the stable Indian margin of

Gondwana, whereas the Upper Permian strata are derived from the active South Qiangtang Terrane (Fig. 7). The sedimentary provenance changed significantly between the Late Carboniferous–Early Permian and Late Permian periods. The angular unconformity between the Lower Permian Tunlonggongba and Upper Permian Jipuria formations in the Ritu area (Fig. 2; Liang et al., 1983; Zhang et al., 2019) indicate that the western South Qiangtang Terrane must have been uplifted after deposition of the Lower Permian Tunlonggongba Formation, which marks the point at which the provenance changed (Figs. 2, 7). The same observations (Figs. 2, 7) further suggest that the provenance change may have started in the Early Permian (ca. 280 Ma), and continued into the Middle Permian (273–260 Ma).

### 5.3. Cause of the 280–260 Ma sedimentary provenance change in the South Qiangtang Terrane

The cause of the 280–260 Ma sedimentary provenance change in the South Qiangtang Terrane is debated. Extensive magmatism occurred at 300–279 Ma in South Qiangtang, Baoshan, Himalayas and Panjal along the northern Indian margin of Gondwana, over an area greater than  $2 \times 10^6 \text{ km}^2$  (Zhai et al., 2013; Zhu et al., 2013; Shellnutt et al., 2014; Liao et al., 2015; Wang et al., 2019). This magmatism is characterised by mafic dike swarms and basalts (Zhai et al., 2013; Wang et al., 2014; Fig. 1b). Whole-rock geochemical data indicate that the mafic dike swarms are tholeiitic in composition, exhibit relative enrichment in light rare earth elements, and have high Nb, Ta and Ti contents, which is typical of intra-plate basalts (Zhai et al., 2013; Wang et al., 2014, 2019; Liao et al., 2015). They show consistently positive  $\varepsilon\text{Nd(t)}$  (e.g., +2.3 to +7.6 in the South Qiangtang Terrane) and  $\varepsilon\text{Hf(t)}$  (e.g., +4.2 to +15.8 in the South Qiangtang Terrane; Zhai et al., 2013; Wang et al., 2019) values. These results indicate that the 300–279 Ma magmatism was most likely derived from an enriched subcontinental lithospheric mantle source and triggered by the mantle plume-induced rifting process occurring on the northern Indian margin of Gondwana (Zhai et al., 2013; Wang et al., 2014, 2019; Liao et al., 2015).

The 280–260 Ma sedimentary provenance change in the South Qiangtang Terrane closely follows the 300–279 Ma rifting magmatism in time and space. We infer that the 280–260 Ma sedimentary provenance change in the South Qiangtang Terrane was caused by the widespread 300–279 Ma rifting magmatism. This process resulted in uplift of the northern Indian margin of Gondwana (e.g., the South Qiangtang) and a change of depositional environment from marine to terrestrial at 280–260 Ma (Figs. 2, 7). This uplift resulted in erosion of Ordovician, Late Devonian–Early Carboniferous and Permian magmatic and sedimentary rocks, which changed the sedimentary provenance signature of the area significantly.

The rifting magmatism at 300–279 Ma may represent the early stage of rifting, and the 280–260 Ma sedimentary provenance change may represent the late stage (Fig. 8). The rifting magmatism and subsequent sedimentary provenance change represent a complete Early–Middle

Permian (300–260 Ma) rifting process on the northern Indian margin of Gondwana.

### 5.4. Opening of the Meso-Tethys Ocean

The opening of the Meso-Tethys Ocean was genetically the rifting of the South Qiangtang Terrane from the Indian margin of Gondwana (Yin and Harrison, 2000; Metcalfe, 2013; Zhai et al., 2013; Liao et al., 2015; Chen et al., 2017). The Early–Middle Permian (300–260 Ma) rifting process on the northern Indian margin of Gondwana (e.g., the South Qiangtang) may represent the initial opening of the Meso-Tethys Ocean. This interpretation is also supported by the following three lines of evidence.

- (1) The parent material of the Late Carboniferous–Early Permian glacial marine diamictites and sandstones (ca. 300 Ma) in the South Qiangtang Terrane was derived directly from the Indian margin of Gondwana (Fig. 7; Fan et al., 2015). This indicates that the South Qiangtang Terrane was still connected to the Indian margin of Gondwana at least during the Late Carboniferous–Early Permian (ca. 300 Ma; Fig. 9a). The initial opening of the Meso-Tethys must have occurred after this time.
- (2) The ages of the oldest MORB-type and OIB-type ophiolites in the BNSZ are Late Permian–Early Triassic (260–250 Ma; Huang et al., 2012; Wang et al., 2015b; Dong et al., 2016; Zhang et al., 2016, 2017) indicating that development of the Meso-Tethys oceanic crust occurred during this period. The 300–279 Ma rifting magmatism marks the early stage of the rifting process (Figs. 8, 9b; Metcalfe, 2013; Liao et al., 2015; Chen et al., 2017; Wang et al., 2019) and the 280–260 Ma sedimentary provenance change marks the late stage (Figs. 8, 9c). The 260–250 Ma ophiolites in the BNSZ represent the oceanic crust after ocean opening (Figs. 8, 9d). From earliest to latest, the 300–279 Ma rift magmatism, 280–260 Ma sedimentary provenance change, and 260–250 Ma ophiolites complete the geological record of the rifting to opening process of the Meso-Tethys Ocean (Fig. 8), which provides strong evidence that the Meso-Tethys Ocean opened during the Early–Middle Permian (300–260 Ma).
- (3) Previous paleontological studies have shown that a significant paleobiogeographic change from a peri-Gondwanan to transitional affinity (the Tethyan Cimmerian subregion) occurred in the South Qiangtang Terrane from the Artinskian to the Kungurian (Zhang et al., 2012b, 2014b; Shen et al., 2016). This transition was the result of the effects of the northward drift of the South Qiangtang Terrane (Zhang et al., 2012b), which provides further evidence that the opening of the Meso-Tethys Ocean occurred during Early–Middle Permian (300–260 Ma).

## 6. Conclusions

- (1) A significant change in sedimentary provenance occurred between 280 and 260 Ma in the South Qiangtang Terrane of the Tibetan Plateau.
- (2) The 280–260 Ma provenance change is associated with the development of the rift-related magmatism at 300–279 Ma on the northern Indian margin of Gondwana (e.g., South Qiangtang).
- (3) The 300–279 Ma magmatism and the subsequent 280–260 Ma sedimentary provenance change represent a complete Early–Middle Permian (300–260 Ma) rifting process, which marks the opening of the Meso-Tethys Ocean.

## Declaration of competing interest

We declare that we have no financial and personal relationships with other people or organizations that can appropriately influence our work; there is no professional or other personal interest of any nature or

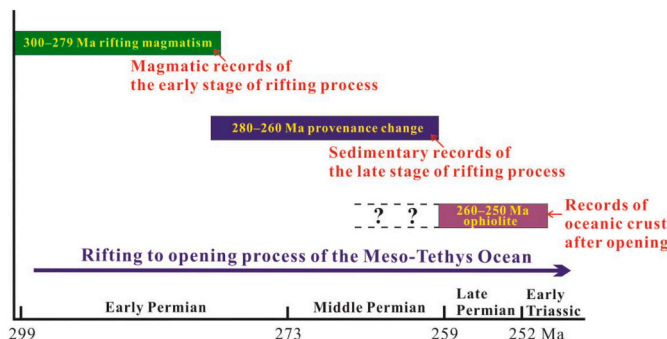


**Fig. 8.** Permian geological records showing the rifting to opening process of the Meso-Tethys Ocean.

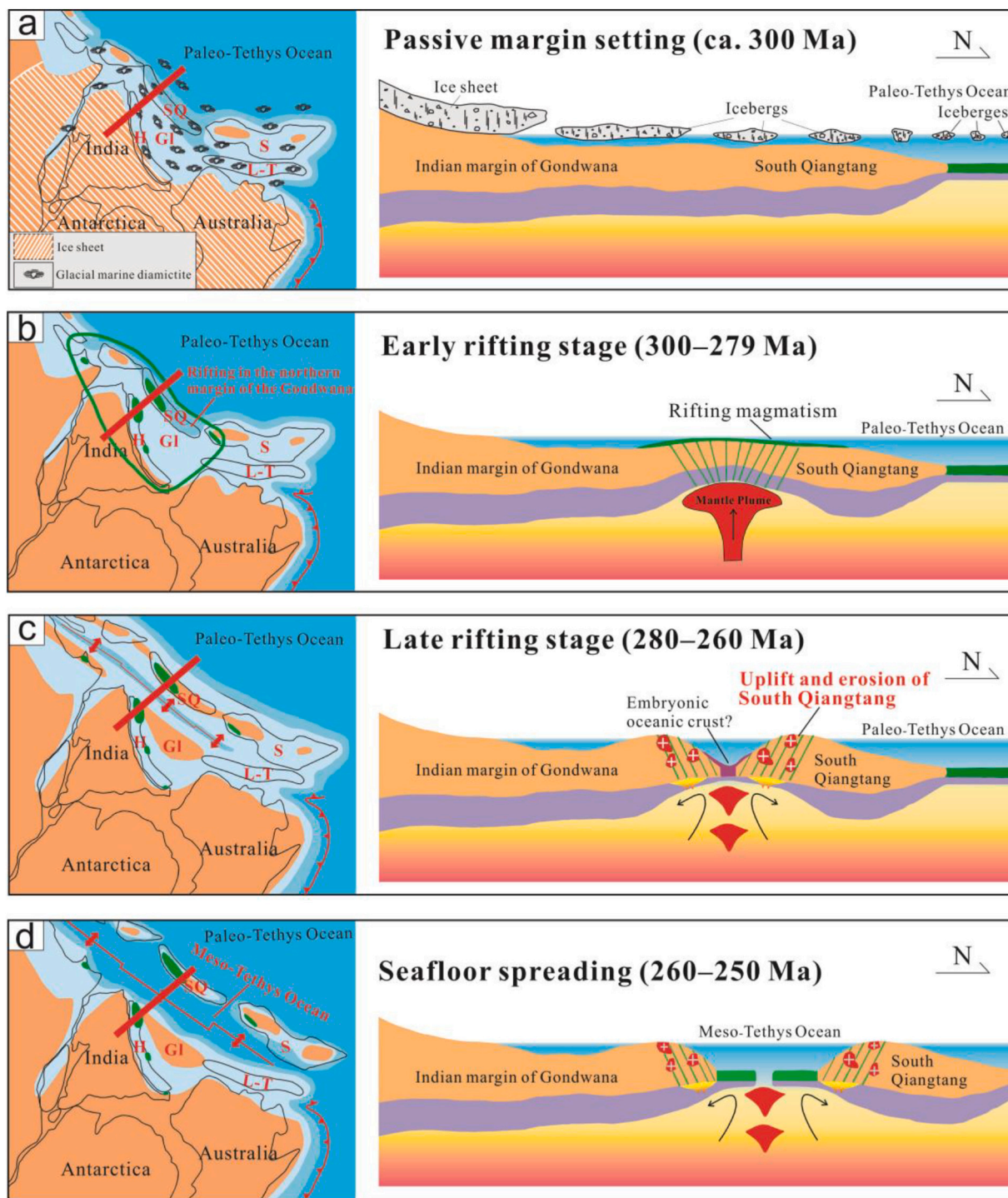


**Fig. 9.** Schematic model showing the opening process of the Meso-Tethys (modified after Torsvik and Cocks, 2013; Metcalfe, 2013; Zhai et al., 2013; Liao et al., 2015; Chen et al., 2017; Wang et al., 2019). H, Himalayas; L-T, Lhasa-Tengchong; S, Sibumasu; SQ, South Qiangtang; GI, Greater India. Red bars show the cross sections. (For interpretation of the references to colour in this figure legend, the reader is referred to the web version of this article.)

kind in any product; service and/or company that could be construed as influencing the position presented in, or the review of, the manuscript entitled.

#### Acknowledgments

We sincerely thank Xiao-Wen Zeng, Hang Li, Hao Wu, and Yun-Peng Yu for the help in the field. This research was supported by the Second Tibetan Plateau Scientific Expedition and Research Program (STEP;

Grant No. 2019QZKK0703), the National Science Foundation of China (Grant Nos. 41972236, 41702227), and Self-determined Foundation of Key Laboratory of Mineral Resources Evaluation in Northeast Asia, Ministry of Natural Resources of China (DBY-ZZ-18-04). All data are provided in the present manuscript and supporting information. The latter includes Figs. S1–2 and Tables S1–5 and is available at <https://zenodo.org/deposit/3754981> (DOI: <https://doi.org/10.5281/zenod.3754981>).

## Appendix A. Supplementary data

Supplementary data to this article can be found online at <https://doi.org/10.1016/j.palaeo.2021.110265>.

## References

- Allègre, C.J., Courtillot, V., Tapponnie, P., 1984. Structure and evolution of the Himalaya-Tibet orogenic belt. *Nature* 307 (p), 17–22.
- Anderson, T., 2002. Correction of common lead in U-Pb analyses that do not report  $^{204}\text{Pb}$ . *Chem. Geol.* 192, 59–79.
- Cawood, P.A., Hawkesworth, C.J., Dhuime, B., 2012. Detrital zircon record and tectonic setting. *Geology* 40, 875–878.
- Chen, S.S., Shi, R.D., Fan, W.M., Gong, X.H., Wu, K., 2017. Early Permian mafic dikes in the Nagqu area, Central Tibet, China, associated with embryonic oceanic crust of the Meso-Tethys Ocean. *J. Geophys. Res. Solid Earth* 122, 4172–4190.
- Dickinson, W.R., 1985. Interpreting provenance relations from detrital modes of sandstones. In: Provenance of Arenites. Springer, pp. 333–361.
- Dickinson, W., Gehrels, G., 2009. Use of U-Pb ages of detrital zircons to infer maximum depositional ages of strata: a test against a Colorado Plateau Mesozoic database. *Earth Planet. Sci. Lett.* 288, 115–125.
- Dong, Y.L., Wang, B.D., Zhao, W.X., Tang, T.N., Xu, J.F., 2016. Discovery of eclogite in the Bangong Co-Nujiang ophiolitic mélange, central Tibet, and tectonic implications. *Gondwana Res.* 35, 115–123.
- von Eynatten, H., Dunkl, I., 2012. Assessing the sediment factory: the role of single grain analysis. *Earth Sci. Rev.* 115, 97–120.
- Fan, J.J., Li, C., Wang, M., Xie, C.M., Xu, W., 2015. Features, provenance, and tectonic significance of Carboniferous–Permian glacial marine diamictites in the Southern Qiangtang–Baoshan block, Tibetan Plateau. *Gondwana Res.* 28, 1530–1542.
- Fan, J.J., Li, C., Wang, M., Liu, Y.M., Xie, C.M., 2017. Remnants of a Late Triassic ocean island in the Gufeng area, northern Tibet: Implications for the opening and early evolution of the Bangong–Nujiang Tethyan Ocean. *J. Asian Earth Sci.* 135, 35–50.
- Fan, J.J., Li, C., Wang, M., Xie, C.M., 2018. Reconstructing in space and time the closure of the middle and western segments of the Bangong–Nujiang Tethyan Ocean in the Tibetan Plateau. *Int. J. Earth Sci.* 107, 231–249.
- Fan, J.J., Niu, Y., Liu, Y.M., Hao, Y.J., 2021. Timing of closure of the Meso-Tethys Ocean: Constraints from remnants of a 141–135 Ma ocean island within the Bangong–Nujiang Suture Zone, Tibetan Plateau. *Geol. Soc. Am. Bull.* <https://doi.org/10.1130/B35896.1>.
- Fielding, C.R., Frank, T.D., Isbell, J.L., 2008. Resolving the Late Paleozoic Ice Age in Time and Space: Geological Society of America Special Paper, p. 441.
- Gehrels, G., Kapp, P., DeCelles, P., Pullen, A., Blakey, R., Weislogel, A., Ding, L., Guynn, J., Martin, A., McQuarrie, N., Yin, A., 2011. Detrital zircon geochronology of preTertiary strata in the Tibetan–Himalayan orogeny. *Tectonics* 30, TC5016.
- Geng, Q., Zhang, Z., Peng, Z., Guan, J., Zhu, X., Mao, X., 2016. Jurassic–Cretaceous granitoids and related tectono-metallogenesis in the Zapug–Duobuza arc, western Tibet. *Ore Geol. Rev.* 77, 163–175.
- Goolaerts, A., Mattielli, N., de Jong, J., Weis, D., Scoates, J.S., 2004. Hf and Lu isotopic reference values for the zircon standard 91500 by MC-ICP-MS. *Chem. Geol.* 206, 1–9.
- Hao, L.L., Wang, Q., Zhang, C., Qu, Q., Yang, J.H., Dan, W., Jiang, Z.Q., 2019. Oceanic plateau subduction during closure of the Bangong–Nujiang Tethyan Ocean: insights from central Tibetan volcanic rocks. *Geol. Soc. Am. Bull.* 131, 864–880.
- Hu, Z.C., Liu, Y.S., Gao, S., Liu, W.G., Zhang, W., Tong, X.R., Lin, L., Zong, K.Q., Li, M., Chen, H.H., Zhou, L., Yang, L., 2012. Improved in situ Hf isotope ratio analysis of zircon using newly designed X skimmer cone and Jet sample cone in combination with the addition of nitrogen by laser ablation multiple collector ICP-MS. *J. Anal. At. Spectrom.* 27, 1391–1399.
- Hu, P.Y., Zhai, Q.G., Jahn, B.M., Wang, J., Li, C., Lee, H.Y., Tang, S.H., 2015. Early Ordovician granites from the South Qiangtang terrane, northern Tibet: Implications for the early Paleozoic tectonic evolution along the Gondwanan proto-Tethyan margin. *Lithos* 220–223, 318–338.
- Hu, P.Y., Zhai, Q.G., Jahn, B.M., Wang, J., Chung, S.L., Lee, H.Y., Tang, S.H., 2017. Late Early Cretaceous magmatic rocks (118–113 Ma) in the middle segment of the Bangong–Nujiang suture zone, Tibetan Plateau: evidence of lithospheric delamination. *Gondwana Res.* 44, 116–138.
- Huang, Q.S., Shi, R.D., Ding, B.H., Liu, D.L., Zhang, X.R., Fan, S.Q., Zhi, X.C., 2012. Re-Os isotopic evidence of MOR-type ophiolite from the Bangong Co for the opening of Bangong–Nujiang Tethys Ocean. *Acta Petrol. Mineral.* 21, 465–478 (in Chinese with English abstract).
- Ingersoll, R.V., Bullard, T.F., Ford, R.L., Grimm, J.P., Pickle, J.D., Sares, S.W., 1984. The effect of grain size on detrital modes: a test of the Gazzi-Dickinson point-counting method. *J. Sediment. Res.* 54, 103–116.
- Jin, X.C., 2002. Carboniferous–Permian sequences of Gondwana affinity in southwest China and their paleogeographic implications. *J. Asian Earth Sci.* 20, 633–646.
- Kapp, P., DeCelles, P.G., Gehrels, G.E., Heizler, M., Ding, L., 2007. Geological records of the Lhasa–Qiangtang and Indo–Asian collisions in the Nima area of central Tibet. *Geol. Soc. Am. Bull.* 119, 917–932.
- Li, J.X., Qin, K.Z., Li, G.M., Richards, J.P., Zhao, J.X., Cao, M.J., 2014. Geochronology, geochemistry, and zircon Hf isotopic compositions of Mesozoic intermediate–felsic intrusions in central Tibet: petrogenetic and tectonic implications. *Lithos* 198–199, 77–91.
- Li, X.K., Chen, J., Wang, R.C., Li, C., 2018. Temporal and spatial variations of Late Mesozoic granitoids in the SW Qiangtang, Tibet: Implications for crustal architecture, Meso-Tethyan evolution and regional mineralization. *Earth Sci. Rev.* 185, 374–396.
- Li, S., Yin, C., Guilmette, C., Ding, L., Zhang, J., 2019. Birth and demise of the Bangong–Nujiang Tethyan Ocean: a review from the Gerze area of central Tibet. *Earth Sci. Rev.* 198, 102907.
- Li, S.M., Wang, Q., Zhu, D.C., Cawood, P.A., Stern, R.J., Weinberg, R., Zhao, Z.D., Mo, X., 2020. Reconciling Orogenic Drivers for the Evolution of the Bangong–Nujiang Tethys during Middle-Late Jurassic. *Tectonics* 39 e2019TC005951.
- Liang, D.Y., Nie, Z.T., Guo, T.Y., Xu, B.W., Zhang, Y.Z., Wang, J.P., 1983. Perm-Carboniferous Gondwana-Tethys facies in southern Karakoram Ali, Xizang (Tibet). *Earth Sci.* 19, 9–27 (in Chinese with English abstract).
- Liang, X., Sun, X., Wang, G., Gao, J., An, X., 2020. Sedimentary evolution and provenance of the late Permian-middle Triassic Raggyorcaka deposits in North Qiangtang (Tibet, Western China): evidence for a Forearc basin of the Longmu Co-Shuanghu Tethys Ocean. *Tectonics* 39 e2019TC005589.
- Liao, S.Y., Wang, D.B., Tang, Y., Yin, F.G., Cao, S.N., Wang, L.Q., Wang, B.D., Sun, Z.M., 2015. Late Paleozoic Woniusi basaltic province from Sibumasu terrane: implications for the breakup of eastern Gondwana's northern margin. *Geol. Soc. Am. Bull.* 127, 1313–1330.
- Liu, B.P., Cui, X.S., 1983. Discovery of Eurydesma-fauna from Rutog, northwest Xizang (Tibet), and its biogeographic significance. *Earth Sci. J. Wuhan Coll. Geol.* 19, 79–92 (in Chinese with English abstract).
- Liu, Y.S., Gao, S., Hu, Z.C., Gao, C.G., Zong, K.Q., Wang, D.B., 2010. Continental and oceanic crust recycling-induced melt–peridotite interactions in the Trans–North China Orogen: U-Pb dating, Hf isotopes and trace elements in zircons from mantle xenoliths. *J. Petrol.* 51, 537–571.
- Liu, D., Shi, R., Ding, L., Huang, Q., Zhang, X., Yue, Y., Zhang, L., 2017. Zircon U-Pb age and Hf isotopic compositions of Mesozoic granitoids in southern Qiangtang, Tibet: implications for the subduction of the Bangong–Nujiang Tethyan Ocean. *Gondwana Res.* 41, 157–172.
- Liu, Y., Li, S., Santosh, M., Cao, H., Yu, S., Wang, Y., Zhou, J., Zhou, Z., 2019. The generation and reworking of continental crust during early Paleozoic in Gondwanan affinity terranes from the Tibet Plateau. *Earth Sci. Rev.* 190, 486–497.
- Ludwig, K.J., 2003. ISOPLOT 3.0, Berkeley Geochronology Center Special Publication, p. 70.
- Luo, A.B., Fan, J.J., Hao, Y.J., Li, H., Zhang, B.C., 2020. Aptian Flysch in central Tibet: constraints on the timing of closure of the Bangong–Nujiang Tethyan ocean. *Tectonics* 39 e2020TC006198.
- Ma, A., Hu, X., Garzanti, E., Han, Z., Lai, W., 2017. Sedimentary and tectonic evolution of the southern Qiangtang basin: Implications for the Lhasa–Qiangtang collision timing. *J. Geophys. Res. Solid Earth* 122, 4790–4813.
- Malusa, M.G., Villa, I.M., Vezzoli, G., Garzanti, E., 2011. Detrital geochronology of unroofing magmatic complexes and the slow erosion of oligocene volcanoes in the Alps. *Earth Planet. Sci. Lett.* 301, 324–336.
- Metcalf, I., 2013. Gondwana dispersion and Asian accretion: tectonic and palaeogeographic evolution of eastern Tethys. *J. Asian Earth Sci.* 66, 1–33.
- Mou, S.Y., Wang, C.W., Wang, M., Chen, R., Zeng, C.X., 2010. 1:250000 Geological Survey Report of Nagqu County. China University of Geosciences Press, Tibet, Wuhan (in Chinese).
- Nie, Z.T., Song, Z.M., 1983a. Fusulinids of lower Permian Qudi formation from Rutog of Xizang (Tibet), China. *Earth Sci. J. China Univ. Geosci.* 29–42 (in Chinese with English abstract).
- Nie, Z.T., Song, Z.M., 1983b. Fusulinids of Lower Permian Tunlonggongba formation from Rutog of Xizang. *Earth Sci. J. Wuhan Coll. Geol.* 19, 43–55 (in Chinese with English abstract).
- Nie, Z.T., Song, Z.M., 1983c. Fusulinids of Lower Permian Maokouan Longge formation from Rutog, Xizang (Tibet), China. *Earth Sci. J. Wuhan Coll. Geol.* 19, 57–68 (in Chinese with English abstract).
- Pan, G.T., Wang, L.Q., Li, R.S., Yuan, S.H., Ji, W.H., Yin, F.G., Zhang, W.P., Wang, B.D., 2012. Tectonic evolution of the Qinghai–Tibet Plateau. *J. Asian Earth Sci.* 53, 3–14.
- Shellnutt, J.G., Bhat, G.M., Wang, K.L., Brookfield, M.E., Jahn, B.M., Dostal, J., 2014. Petrogenesis of the flood basalts from the Early Permian Panjal Traps, Kashmir, India: Geochemical evidence for shallow melting of the mantle. *Lithos* 204, 159–171.
- Shen, S.Z., Sun, T.R., Zhang, Y.C., Yuan, D.X., 2016. An upper Kunjurang/lower Guadalupian (Permian) brachiopod fauna from the South Qiangtang Block in Tibet and its palaeobiogeographical implications. *Palaeoworld* 25, 519–538.
- Shi, R.D., Yang, J.S., Xu, Z.Q., Qi, X.X., 2008. The Bangong Lake ophiolite (NW Tibet) and its bearing on the tectonic evolution of the Bangong–Nujiang suture zone. *J. Asian Earth Sci.* 32, 438–457.
- Tang, Y., Zhai, Q.G., Chung, S.L., Hu, P.Y., Wang, J., Xiao, X.C., Song, B., Wang, H.T., Lee, H.Y., 2020. First mid-ocean ridge-type ophiolite from the Meso-Tethys suture zone in the north-central Tibetan plateau. *Geol. Soc. Am. Bull.* 132, 2202–2220.
- Torsvik, T.H., Cocks, L.R.M., 2013. Gondwana from top to base in space and time. *Tectonophysics* 24, 999–1030.
- Wang, M., Li, C., Wu, Y.W., Xie, C.M., 2014. Geochronology, geochemistry, Hf isotopic compositions and formation mechanism of radial mafic dikes in northern Tibet. *Int. Geol. Rev.* 56, 187–205.
- Wang, M., Li, C., Xie, C.M., Xu, J.X., Li, X.K., 2015a. U-Pb zircon age, geochemical and Lu-Hf isotopic constraints of the Southern Gangma Co basalts in the Central Qiangtang, northern Tibet. *Tectonophysics* 657, 219–229.
- Wang, B.D., Wang, L.Q., Xu, J.F., Chen, L., Zhao, W.X., Liu, H., Peng, T.P., Li, X.B., 2015b. The discovery of high-pressure granulite at Shela Ma in Dongco area along the Bangong Co-Nujiang River suture zone and its tectonic significance. *Geol. Bull. China* 34, 1605–1616 (in Chinese with English abstract).
- Wang, B.D., Wang, L.Q., Chung, S.L., Chen, J.L., Yin, F.G., Liu, H., Li, X.B., Chen, L.X., 2016. Evolution of the Bangong–Nujiang Tethyan ocean: insights from the

- geochronology and geochemistry of mafic rocks within ophiolites. *Lithos* 245, 18–33.
- Wang, M., Li, C., Zeng, X.W., Li, H., Fan, J.J., Xie, C.M., Hao, Y.J., 2019. Petrogenesis of the southern Qiangtang mafic dykes, Tibet: link to a late Paleozoic mantle plume on the northern margin of Gondwana? *Geol. Soc. Am. Bull.* 131, 1907–1919.
- Wiedenbeck, M., Allé, P., Corfu, F., Griffin, W.L., Meier, M., Oberli, F., Quadat, A.V., Roddick, J.C., Spiegel, W., 1995. Three natural zircon standards for U–Th–Pb, Lu–Hf, trace element and REE analyses. *Geostand. Geoanal. Res.* 19, 1–23.
- Woodhead, J., Herget, J., Shelley, M., Eggin, S., Kemp, R., 2004. Zircon Hf-isotope analysis with an excimer laser, depth profiling, ablation of complex geometries, and concomitant age estimation. *Chem. Geol.* 209, 121–135.
- Wu, R.Z., Lan, B.L., 1990. New Late Permian strata from Northwest Tibet. *J. Stratigr.* 14, 216–221 (in Chinese with English abstract).
- Wu, H., Sun, S., Liu, H., Chu, H., Ding, W., 2018. An Early Cretaceous slab window beneath central Tibet, SW China: evidence from OIB-like alkaline gabbros in the Duolong area. *Terra Nova* 31, 67–75.
- Xia, D.X., Liu, S.S., 1997. The Lithostratigraphy of the Tibet. Publishing House of China University of Geosciences (In Chinese).
- Xie, C.M., Li, C., Fan, J.J., Su, L., 2017. Ordovician sedimentation and bimodal volcanism in the Southern Qiangtang terrane of northern Tibet: implications for the evolution of the northern Gondwana margin. *Int. Geol. Rev.* 59, 2078–2105.
- Xu, Z., Dilek, Y., Cao, H., Yang, J., Robinson, P., Ma, C., Li, H., Jolivet, M., Roger, F., Chen, X., 2015. Paleo-Tethyan evolution of Tibet as recorded in the East Cimmerides and West Cathaysides. *J. Asian Earth Sci.* 105, 320–337.
- Xu, W., Liu, F., Dong, Y., 2020. Cambrian to Triassic geodynamic evolution of central Qiangtang, Tibet. *Earth Sci. Rev.* 201, 103083.
- Yin, A., Harrison, T.M., 2000. Geologic evolution of the Himalayan–Tibetan orogeny. *Annu. Rev. Earth Planet. Sci.* 28, 211–280.
- Yuan, H.L., Gao, S., Liu, X.M., Li, H.M., Günther, D., Wu, F.Y., 2004. Accurate U–Pb age and trace element determinations of zircon by laser ablation-inductively coupled plasma mass spectrometry. *Geostand. Geoanal. Res.* 28, 353–370.
- Zeng, Y.C., Chen, J.L., Xu, J.F., Wang, B.D., Huang, F., 2016. Sediment melting during subduction initiation: geochronological and geochemical evidence from the Darutso high-Mg andesites within ophiolite melange, central Tibet. *Geochem. Geophys. Geosyst.* 17, 4859–4877.
- Zhai, Q.G., Jahn, B.M., Su, L., Ernst, R.E., Wang, K.L., Zhang, R.Y., Wang, J., Tang, S.H., 2013. SHRIMP zircon U–Pb geochronology, geochemistry and Sr–Nd–Hf isotopic compositions of a mafic dyke swarm in the Qiangtang terrane, northern Tibet and geodynamic implications. *Lithos* 174, 28–43.
- Zhai, Q.G., Jahn, B.M., Wang, J., Hu, P.Y., Chung, S.L., Lee, H.Y., Tang, S.H., Tang, Y., 2016. Oldest Paleo-Tethyan ophiolitic mélange in the Tibetan Plateau. *Geol. Soc. Am. Bull.* 128, 355–373.
- Zhang, Y.C., Shen, S.Z., Shi, G.R., Wang, Y., Yuan, D.X., Zhang, Y.J., 2012a. Tectonic evolution of the Qiangtang Block, northern Tibet during the Late Cisuralian (Late Early Permian): evidence from fusuline fossil records. *Palaeogeogr. Palaeoclimatol. Palaeoecol.* 350–352, 139–148.
- Zhang, Y.C., Wang, Y., Zhang, Y.J., Yuan, D.X., 2012b. Kungurian (Late Cisuralian) fusuline fauna from the Cuozheqiangma area, northern Tibet and its palaeobiogeographical implications. *Palaeoworld* 21, 139–152.
- Zhang, Y.C., Shi, G.R., Shen, S.Z., 2013. A review of Permian stratigraphy, palaeobiogeography and palaeogeography of the Qinghai–Tibet Plateau. *Gondwana Res.* 24, 55–76.
- Zhang, K.J., Xia, B., Zhang, Y.X., Liu, W.L., Zeng, L., Li, J.F., Xu, L.F., 2014a. Central Tibetan Meso-Tethyan oceanic plateau. *Lithos* 210–211, 278–288.
- Zhang, Y.C., Shi, G.R., Shen, S.Z., Yuan, D.X., 2014b. Permian Fusuline Fauna from the lower part of the Lugu Formation in the Central Qiangtang Block and its geological implications. *Acta Geo. Sin.* 88, 365–379.
- Zhang, Y.X., Li, Z.M., Zhu, L.D., Zhan, K.J., Yang, W.G., Jin, X., 2016. Newly discovered eclogites from the Bangong Meso-Tethyan suture zone (Gaize, central Tibet, western China): mineralogy, geochemistry, geochronology, and tectonic implications. *Int. Geol. Rev.* 58, 574–587.
- Zhang, X.Z., Wang, Q., Dong, Y.S., Zhang, C., Li, Q.Y., Xia, X.P., Xu, W., 2017. High pressure granulite-facies overprinting during the exhumation of eclogites in the Bangong–Nujiang suture zone, central Tibet: link to flat-slab subduction. *Tectonics* 36, 2918–2935.
- Zhang, Y.C., Zhang, Y.J., Yuan, D.X., Xu, H.P., Qiao, F., 2019. Stratigraphic and paleontological constraints on the opening time of the Bangong-Nujiang Ocean. *Acta Petrol. Sin.* 35, 3083–3096 (in Chinese with English abstract).
- Zhu, D.C., Zhao, Z.D., Niu, Y., Dilek, Y., Hou, Z.Q., Mo, X.X., 2013. The origin and pre-Cenozoic evolution of the Tibetan Plateau. *Gondwana Res.* 23, 1429–1454.
- Zhu, D.C., Li, S.M., Cawood, P.A., Wang, Q., Zhao, Z.D., Liu, S.A., Wang, L.Q., 2016. Assembly of the Lhasa and Qiangtang terranes in central Tibet by divergent double subduction. *Lithos* 245, 7–17.